Seismic monitoring of a simulated rockburst on a wall of an underground tunnel

by A.M. Milev*, S.M. Spottiswoode*, A.J. Rorke†, and G.J. Finnie‡

Synopsis

A simulated rockburst was conducted underground at Kopanang Mine, previously called Vaal Reefs No. 9 Shaft. The rockburst was simulated by means of a large blast detonated in solid rock close to a crosscut sidewall. The simulated rockburst involved the design of the seismic source, seismic observations in the near and far field, high-speed video filming, a study of rock mass conditions such as fractures, joints, rock strength etc. Knowledge of the site conditions before and after the simulated rockburst was also gained. Some of the important findings are listed below:

- Two areas of damage were identified on the blasting wall: (i) an area of high-intensity damage in which ground velocities of 3.3 m/s were recorded by an accelerometer, which was subsequently ejected in a block of rock, (ii) an area of low-intensity damage where ground velocities of 1.6 m/s were recorded by an accelerometer which remained on the tunnel wall.
- High-speed filming revealed rock fragments being ejected from the wall at velocities in the range of 0.6 m/s to 2.5 m/s. The measurements were taken in the area of low-intensity damage. As planned, no gas pressure was directly involved in damaging the wall of the tunnel.
- The attenuation of peak particle velocities for the main blast in the near field (6 m to 30 m), as a function of distance R, was found to be proportional to $R^{-1.7}$.
- The simulated rockburst was recorded as a local magnitude M_L = 1.3 by the Klerksdorp regional seismic network.
- Peak particle velocities from nearby blasting, recorded on the tunnel wall after the simulated rockburst, were about six times greater then peak particle velocities recorded from the same source area before the simulated rockburst.

Introduction

Underground mining operations are unavoidably associated with damage to the surrounding rock environment. The severity of rockburst damage often varies greatly over small distances. One panel in a longwall may be severely damaged, while an adjacent panel (perhaps even closer to the focus of the seismic event) is unscathed. The vast majority of casualties are caused by the ejection or fall of slabs less than 1.6 m in thickness, (Roberts[1]).

The damage to the underground excavation strongly depends on the following factors: seismic source mechanism, the rockburst damage mechanism, and the site response. The source mechanism refers to phenomena associated with the failure of the rocks mass, often at a pre-existing weakness such as a fault or dyke, which releases seismic energy. When the seismic waves radiated by the source interact with an excavation, the motion of the skin may vary greatly due to numerous factors such as the geometry of the cavity, effect of support systems, and the degree of fracturing. This variability is termed the site response. In situations where the hanging or sidewall collapses or the face bursts, the term rockburst damage mechanism is used to refer to these phenomena. It is believed that a better understanding of these phenomena will enable areas, which have a high potential for sustaining rockburst damage to be identified, and provide design criteria for support systems. In some cases part of the excavations lies within the near field of seismic source and so the source and the damage mechanism can not be really separated. The current level of rockburst studies is limited by the lack of strong ground motion data recorded in the immediate vicinity of large seismic sources. Jesenak *et al.*[2] commented: 'Many investigators have developed direct relationships between damage levels and ground motion parameters. However, difficulties resulting from highly subjective assessment criteria and incomplete or questionable peak ground motion data severely limit the applicability of these relationships. This limitation will only be

* *CSIR: Division of Mining Technology, Auckland Park, South Africa.*

† *Bulk Mining Explosives, Bryanston, South Africa.*

‡ *Department of Chemical Engineering, Technikon Northern Gauteng, South Africa.*

 SA ISSN 0038–223X/3.00 + 0.00. Paper received Feb. 2001; revised paper received Aug. 2001.

overcome when high quality strong ground motion data has been collected and properly analysed'.

This paper describes the simulation of a rockburst by means of a large underground explosion. The following stages were involved in the simulated rockburst: the design of the seismic source, the installation of a micro-seismic array and seismic monitoring, high-speed video filming, and a study of rock mass conditions (fractures, joints, rock strength, etc.) before and after the blast.

Test site and instrumentation

The site is situated at Kopanang mine (previously Vaal Reefs No 9 shaft), Vaal River Operations at the 53 BW23 Crosscut, South. The crosscut is 1600 m below surface.

The lithologies in the crosscut comprise argillaceous quartzites of the Strathmore Formation known locally as the MB2. The quartzites are grey, medium grained and argillaceous. The bases of individual beds are coarser, defining an upward fining sequence. Each bed is usually capped by a dark green argillite up to 5 mm thick. Bedding is generally planar with thicknesses ranging from 50 mm–500 mm. Black argillite lenses occur locally within the quartzites and are laterally impersistent, (Reddy and Spottiswoode[3]).

A N-S trending normal fault dipping 72° to the east occurs 10 m NW from the site. The fault has a throw of over 100 m downthrow to the east. The lithology encountered in the crosscut is thus hangingwall strata of the Vaal Reef. There is some evidence of strike slip movement on the fault.

Five blast holes were drilled from the access crosscut in a direction parallel to the main tunnel. The charged portion of the holes was about 6 m from the tunnel sidewall. The holes were drilled in a vertical plane with the collars about 500 mm apart. The purpose of this design was to exclude gas expansion as a direct source of rock fragmentation. Figure 1 illustrates the underground layout and deployment of seismic sensors.

Three shock type accelerometers were installed close to the projection of the blast on the tunnel wall. Two of them were placed on the sidewall closest to the blast in the area of expected damage and the third one was installed in a nearby borehole 3 m into the hangingwall.

The output of the accelerometers was conditioned using in-line amplifiers. A Speedwave, 4-channel, high-speed digital recorder was used to record the signals. The recorder has a 12 bit resolution and was set at a voltage range of ± 10 V and a sample rate of 500 000 samples per second.

Four Ground Motion Monitors (GMM) comprising 32 geophones were installed along the tunnel. The transducers were placed on the sidewalls, the hangingwall and the footwall. Vertical, horizontal and triaxial boats installed on the skin and into a borehole were used to supply maximum seismic coverage, see Figure 1. Some of the geophones were over-damped with external resistors of 20Ω, 56Ω and 120Ω to improve the dynamic range of the recording system during the blast. The over-damped geophones were calibrated.

Additional assessment of tunnel deformation before and after the simulated rockburst were made using extensometer measurements, ground penetration radar and routine geological techniques such as fracture mapping, assessment of the existing faults and joints and petroscopic observations (Hagan *et al.*[4]). Rock ejection velocities during the blast were filmed using a high-speed video camera.

Calibration blast and pre-blast monitoring

Preliminary modelling, Hildyard and Milev[5] and the use of empirical equations for the calculation of peak particle velocities gave large variations in the expected peak particle

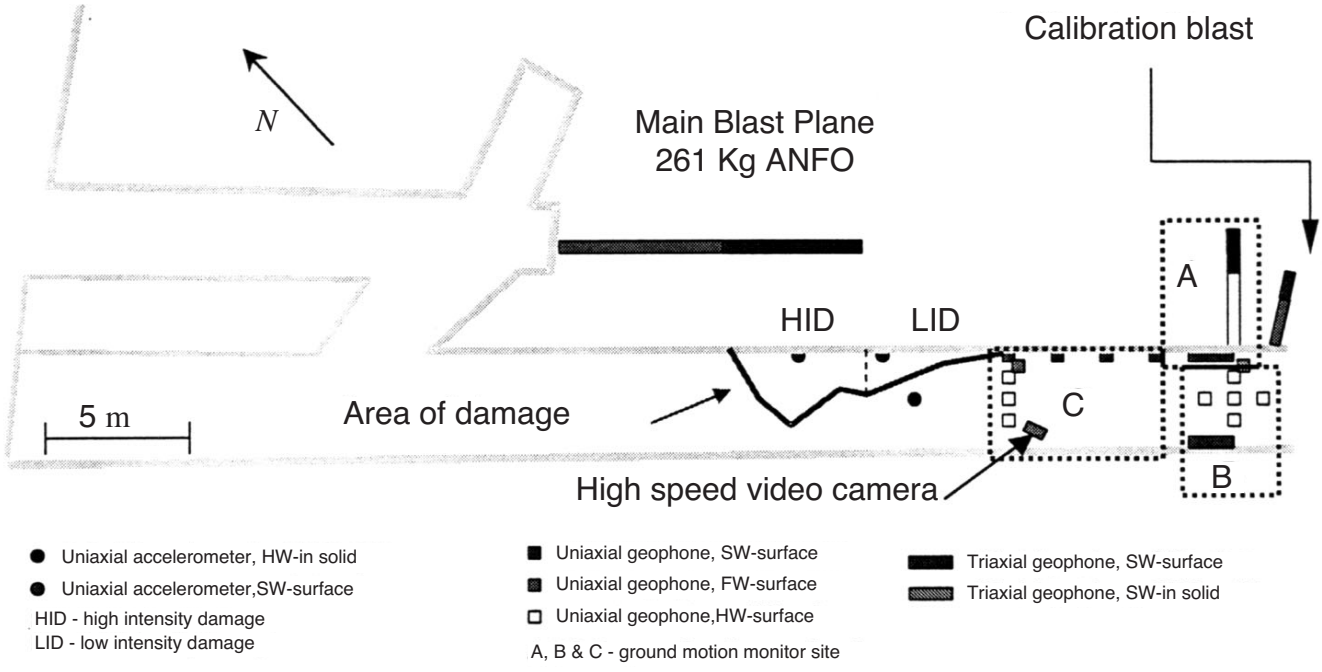

Figure 1—Controlled seismic source experiment layout and deployment of the seismic sensors

velocities. It was therefore decided to perform a small calibration blast.

The blast was conducted into the blasting wall close to the last set of geophones (see Figure 1). A hole, 37 mm in diameter, drilled 75° towards the end of the tunnel, was charged with five 0.12 kg cartridges of Powergell 816. The 0.65 m length charge was stemmed with 1.15 m clay. The estimated Velocity of Detonation (VOD) was 4500 m/s.

The measured values of peak particle velocities (PPVs) from the calibration blast are shown in Figure 2.

The attenuation of peak particle velocities for the calibration blast $A_{(R)}$ as a function of distance R was derived as:

$$A_{(R)} = C\frac{1}{R^{1.1}} \qquad [1]$$

where: C is a constant proportional to the charge mass.

It was important to estimate the parameters of the main blast and predict the position and the value of peak particle velocities on the blasting wall. The charge mass of the calibration blast, Powergell 816, was converted to the equivalent mass ANFO, using 1.1 conversion coefficient. Then the peak particle velocity was estimated as a function of the charge mass Q and the distance R. The following equations have been suggested:

$$PPV = 1143\left(R/Q^{0.5}\right)^{-1.6} \quad [Rorke^{6}] \qquad [2]$$

$$PPV = 650\left(R/Q^{0.5}\right)^{-1.42} \quad [Ouchterlony \text{ et al.}^{7}] \qquad [3]$$

where: R is the distance in metres and Q is the *charge mass* in kilograms.

Persson and Holmberg[8], have scaled Equation [2] for the near field using a scaling factor $f = \text{atan}(H/2R)/(H/2R)$, where H is a charge length in metres

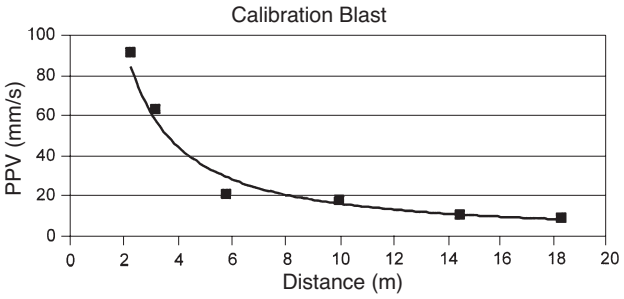

Figure 2—Attenuation curve of peak particle velocities measured from the calibration blast

Table I

The maximum peak particle velocities as a function of charge mass and numbers of holes, according to the Equations [1], [2] and [3]

	Charge mass [kg]	Rorke far field [mm/s]	Ouchterlony far field [mm/s]	Persson and Holmberg near field [mm/s]
1 Hole	40	1664,72	907.48	861.91
2 Holes	80	2898.45	1484.46	1409.91
3 Holes	10	4009.03	1979.68	1880.26
4 Holes	160	5046.50	2428.29	2306.34
5 Holes	200	6032.79	2845.16	2702.28

$$PPV = 650\left(R/fQ^{0.5}\right)^{-1.42}. \qquad [4]$$

The maximum peak particle velocities in respect of the number of holes and the charge mass for 5 m long holes were calculated using Equations [2], [3] and [4] and the results are listed in Table I.

However, these equations are empirically obtained and are based on site-specific measurements. Additional work using numerical modelling was done to estimate the maximum peak particle velocities (Hildyard and Milev[5]).

Main blast

Source description

The purpose of this blast was to simulate a rockburst in a tunnel using explosive energy as a source. However, one fundamental difference between a blast source and dislocation type seismic event is the effect of gas expansion. To prevent direct gas expansion causing ejection, the experimental site was chosen in a crosscut that was intersected by an access crosscut. The holes were drilled in a vertical plane, parallel to the crosscut, with the collars about 0.5 m apart and the distance between the plane and the tunnel sidewall was about 6 m. The exact position of the holes was surveyed relative to the tunnel sidewall.

The holes were charged with 261.5 kg of low density ANFO, using a compressed air loader. Due to mechanical difficulties during the loading of holes 1 and 3, an air gap was left in the end of these holes. The explosive distribution for each hole is given in Table II. The holes were stemmed with quick-setting cement cartridges. The holes were initiated using 10 g/m detonating cord with two Powergell 816 cartridges acting as boosters. The booster position was located 1 m into the charge from the stemming end of the charge. Table II provides a detailed charging report based on the hole length.

Assuming that there were equal lengths of detonating cord down the barrel of each hole, the hole-firing times have been calculated and given in Figure 3. The first hole to fire was the bottom hole. The timing calculation is based on the tie-up of the cord between holes. The cord length was 0.5 m between holes and the detonation velocity of the cord was 7000 m/s.

Table II

Explosive charging details, estimated energies and firing times

Hole number	Hole 1	Hole 2	Hole 3	Hole 4	Hole 5
Explosive type	ANFO	ANFO	ANFO	ANFO	ANFO
Charge Mass/Metre (kg/m)	8.60	8.60	8.60	9.01	9.01
Estimated in-hole density (g/cm^3)	1.05	1.05	1.05	1.10	1.10
Length of stemming (m)	4.80	8.10	3.42	7.30	6.95
Hole Depth (m)	12.30	14.45	13.34	14.45	11.17
Hole Diameter (mm)	102	102	102	102	102
Explosive Mass Per Hole (kg)	49.89	54.62	54.53	64.43	38.03
Estimated explosive VOD (m/s)	3600	3600	3600	3800	3800
Estimated Energy (MJ Per Hole)	126.92	138.96	138.74	163.91	96.74
Estimated Borehole Pressure (GPa)	2.90	2.90	2.90	3.20	3.20
Firing times (μs)	284	213	142	71	0

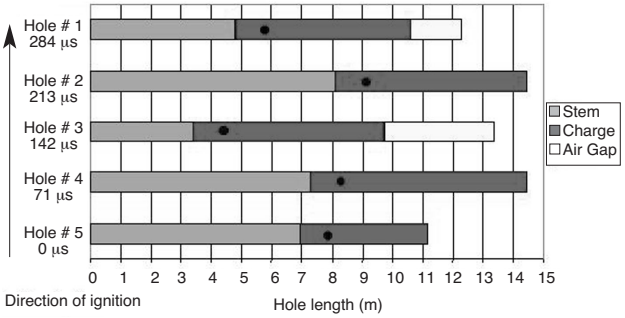

Figure 3—Graphical illustration of the main blast source

A graphical illustration of this explosive source, including length of charge, length of stemming, point of ignition and detonation times, is given in Figure 3.

Seismic observations in the near field

Ground velocities as measured by the accelerometers in the area of damage

Three accelerometers were installed in close proximity to the blast. Two were placed on the sidewall, close to the blast, in the area of expected damage. The third was installed in a borehole 3 m in the hangingwall, to supply a measure of the waves in solid rock (see Figure 1). This accelerometer was also used as a reference for comparison of peak particle velocities recorded in solid rock and on the skin of the tunnel.

The accelerograms recorded in this area are plotted in Figure 4 (a, b, and c).

As the accelerograms developed a DC offset, it was necessary to perform a high-pass filter before the integration to velocity.

The accelerograms were integrated in order to obtain the ground velocities. The peak velocities obtained from accelerometers ACT, ACM and ACH are given in Table III.

The velocity spectra obtained after the integration of accelerograms close to the source are shown in Figure 5. It can be seen that most of the energy recorded in the near field is in the range between 1 kHz and 10 kHz. The spectra shown in Figure 5 are from the accelerometers located in the areas of high-intensity damage and low-intensity damage at the blasting wall, and in the solid rock 3 m into the hangingwall. Note that the spectral shapes for all these points are similar.

The velocity spectra obtained further along the blasting wall recorded by geophones placed at approximately 4 m from each other are shown in Figure 6. Most of the energy recorded at these geophones is in the range of 10 Hz to 110 Hz. This range is much lower than the frequency range obtained for the accelerometers. Two reasons can be pointed out: the rapid attenuation of the higher frequency, or some losses of information due to the lower sampling rate of the Ground Motion Monitor.

The similarity in the spectral shape between the geophones is less than the similarity of the spectral shape between the accelerometers shown in Figure 5.

Ejection velocities from high-speed video camera

A 'Locam' high-speed camera was used to film the tunnel sidewall to measure rock fragment displacement. The position of the camera is shown in Figure 1. The camera is capable of filming at a rate of 500 frames per second. However, lighting conditions in the tunnel were not sufficient; and the frame rate had to be reduced to 200

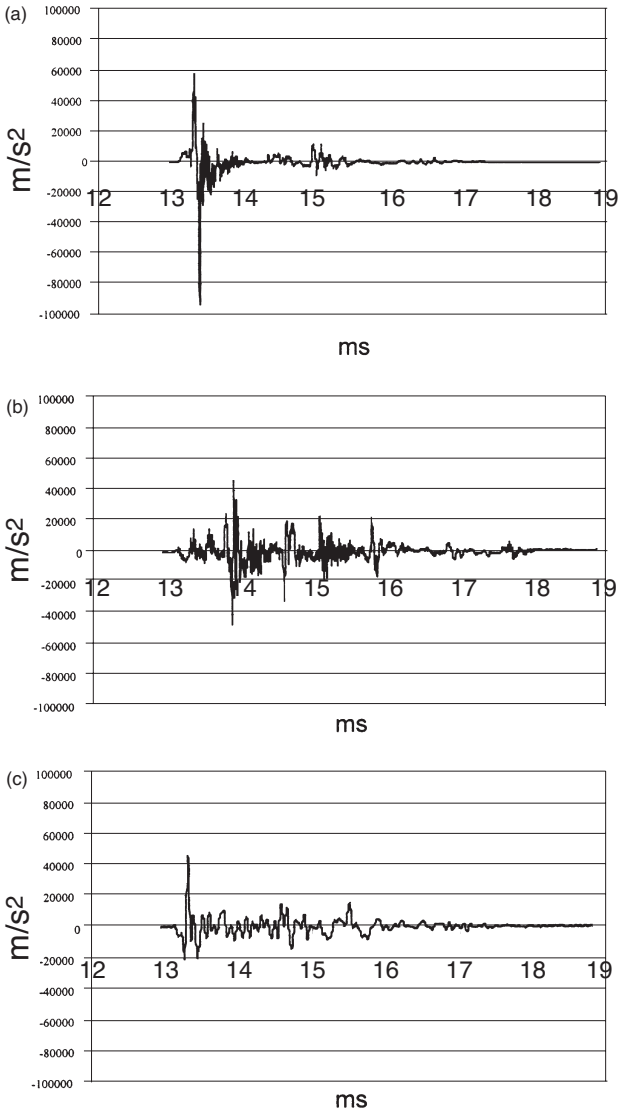

Figure 4 (a, b and c)—Accelerograms recorded in near field: (a) an accelerogram recorded in the area of high-intensity damage (this accelerometer was ejected at 3.3 m/s); (b) an accelerogram recorded in the area of low-intensity damage; (c) an accelerogram recorded in the solid rock 3 m into the hangingwall close to the area of damage

Table III

Velocities obtained from the blasting

Accelerometer	Peak particle velocity (mm/s)	Remarks
ACT	3328	Located in the area of high-intensity damage (HID): ejected
ACM	1626	Located in the area of low-intensity damage (LID): not ejected
ACH	1175	Located in the solid rock, 3 m into the hangingwall: not ejected

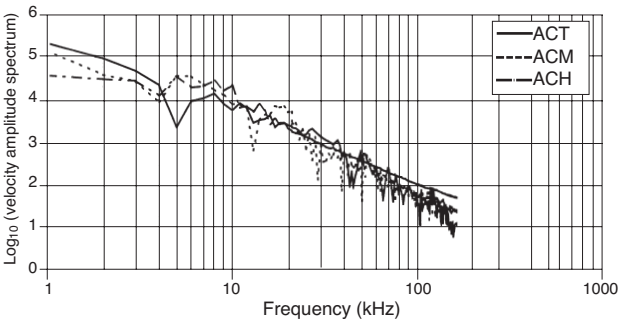

Figure 5—A Log_{10} velocity spectra calculated from the integrated accelerograms, close to the source

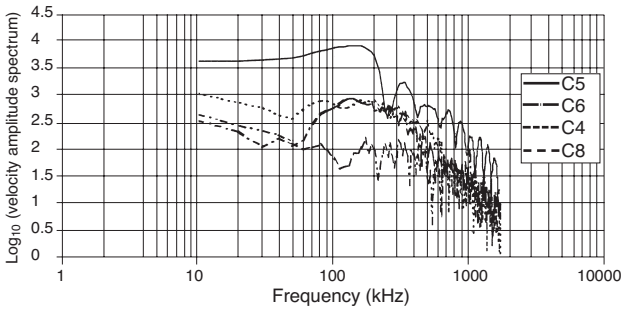

Figure 6—A Log_{10} velocity spectra from the geophones located along the blasting wall

frames per second. This frame rate provided a time resolution of 5 ms per frame.

Nine orange balls were positioned on the tunnel wall closest to the charges. They were located 1 m apart vertically and 2.5 m apart horizontally. The balls were positioned in three vertical sets of three. The first vertical set was located directly opposite the centre of the explosive charges. The second set was located opposite to the end of the charged holes and the third set was located 2.5 m further on. The purpose of the balls was to provide locality information and scaling for the high-speed film.

Due to the insufficient lighting, only the top two balls of the third vertical set could be seen. Displacement recordings given in the following section therefore are related to this position.

The conventional film was converted into VHS videotape and bit mapped computer files.

Fragment velocities were measured by tracking individual fragment positions through space at intervals of 10 frames (equal to 50 ms) at a time. This was done manually by measuring displacements on the projected image and converting these to actual distances using the target ball positions for scaling.

The equation used to convert from the projected image displacement distances to actual displacement distances was:

$$Displacement = \begin{pmatrix} Project\ image \\ displacment \times 8.457 \end{pmatrix} / \cos(14°) \quad [5]$$

The factor 8.457 converts from image pixels to actual distances in mm was obtained by measuring the projected image distance between two marker balls. The angle of the camera to the north wall of the crosscut was 14°. The correction factor cos(14°) was applied because it is assumed the rock fragments were ejected at right angles to the tunnel wall.

The data are plotted in the curves given in Figure 7. Table IV provides a summary of the fitted lines.

For times greater than 100 ms the measurements become random, perhaps due to the interaction of the camera with the other particles or with incoming air waves. In Figure 7 all points above 100 ms have therefore been excluded.

Damage generated from the simulated rockburst

A visual inspection of the damage indicated that no direct gas expansion was involved in the ejection of the rocks.

The volume of blocks ejected per metre of the wall was used to estimate the degree of damage on the blasting wall. Two areas of damage were clearly observed: an area of high intensity damage located opposite of the charges and an area of low intensity damage following towards the end of the tunnel.

The existing support consisted of rock bolt reinforcement showed distortion but not a failure. Most of the rocks were ejected then between the rock bolts. The shape of ejected blocks was determined by the pre-existing bedding separations and stress fractures. Similar interaction between the support of a tunnel and the rock mass, under extreme dynamic loading was observed number of rockburst investigations (Haile[9]).

Attenuation of the PPVs on the blasting wall as a function of distance

The integrated accelerograms and recorded velocities on the

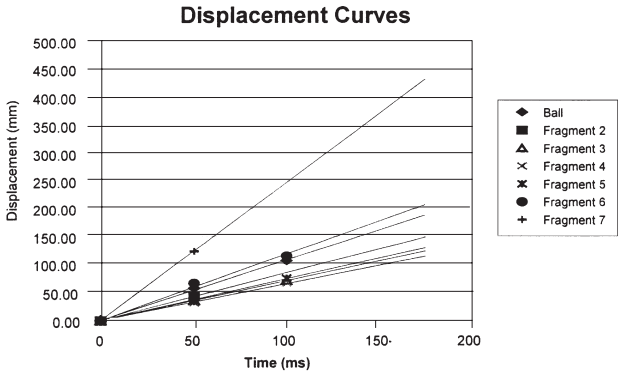

Figure 7—Fitted lines limited to the first 100 ms of data

Table IV

Ejection velocities in m/s obtained from Figure 6

Fragment #	Ejection Velocity (m/s)
Ball	$V_B = 1.145$
Fragment 2	$V_2 = 0.846$
Fragment 3	$V_3 = 0.705$
Fragment 4	$V_4 = 0.617$
Fragment 5	$V_5 = 0.705$
Fragment 6	$V_6 = 1.322$
Fragment 7	$V = 2.467$

blasting wall at sites 'C' and 'A' were plotted as a function of the distance (Figure 8). The distances have been calculated from the centre of gravity of the blast.

The attenuation of peak particle velocities for the main blast $A_{(R)}$ as a function of distance R was found to be:

$$A_{(R)} = C\frac{1}{R^{1.7}} \quad [6]$$

where: C is a constant proportional to the mass of the charge.

Similar values were reported by Ouchterlony *et al.*[7].

The important factors such as joints, faults and number of fractures located in the path of the wave propagation have a strong effect on attenuation. These effects are discussed further in the paragraph 'post-blast measurements'.

PPVs measured in the solid rock and on the skin of the tunnel

Another important issue for the design of underground support resistance to rockbursts is the amplification of the seismic waves at the skin of the excavations. Previous studies have indicated that the seismic waves can be amplified up to 10 times on the fractured and poorly supported surfaces (Durrheim *et al.*[10]; Spottiswoode *et al.*[11] and Milev *et al.*[12]). Two ground motion monitors installed at 30 m from the blast had their transducers placed on the blasting wall, non-blasting wall hangingwall and the footwall. A borehole drilled 5 m into the blasting wall was instrumented with set of triaxial geophones. The position, orientation and the PPVs measured at each of these transducers are given in Table V.

Seismic observations in the far field

The simulated rockburst was recorded by many stations on the Klerksdorp regional seismic network. The local magnitude was estimated as $M_L = 1.3$.

There are significant physical differences in the process of seismic wave generation by blasting and by dislocation source types. In view of this it was important to analyse and compare the structure of the blast seismogram and some of its source parameters recorded in a far field with those generated by dislocation type mining tremors located in adjacent areas.

An example of a three-component seismogram of the blast recorded at about 850 m from the source is given in Figure 9 (a, b and c).

As can be seen from the seismograms, both body wave groups are well developed. However, the portion of the energy radiated into the P-waves is greater (by factor of ten) than the portion of the energy radiated into the S-waves when compared to dislocation type seismic sources (see Figure 10).

An important characteristic of seismic source dynamics is the stress drop, or the difference between the state of stress before and after the rupture. Stress drop can be represented as a plot of *Log E* versus *Log* M_0 (where E is the radiated seismic energy and M_0 is the scalar seismic moment). Figure 11 shows this relationship for the blast and for 14 mining-induced seismic events, which located in the same portion of the mine. Compared to the average event, the regional seismic system recorded a higher ratio of the radiated seismic energy to the seismic moment was obtained for the blast.

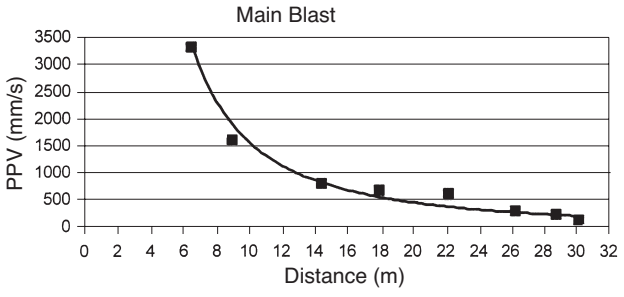

Figure 8–Attenuation curve of peak particle velocities measured from the main blast

Table V

PPVs measured in solid rock, on the skin of the blasting wall

Geophone	Component	Position	PPVs (mm/s)
A2	Radial	Solid/Blasting wall	221
A7	Radial	Skin/Blasting wall	224
B1	Radial	Skin/Non-Blasting wall	145
A6	Transverse	Solid/Blasting wall	77
A8	Transverse	Skin/Blasting wall	135
B2	Transverse	Skin/Non-Blasting wall	95
A4	Vertical	Solid/Blasting wall	82
A5	Vertical	Skin/Blasting wall	160
B4	Vertical	Skin/Non-Blasting wall	142
B5	Vertical	Skin/Hangingwall-edge	155
B6	Vertical	Skin/ Hangingwall-edge	160
B7	Vertical	Skin/Hangingwall-centre	169
B8	Vertical	Skin/Hangingwall-centre	176
A1	Vertical	Skin/Footwall	37

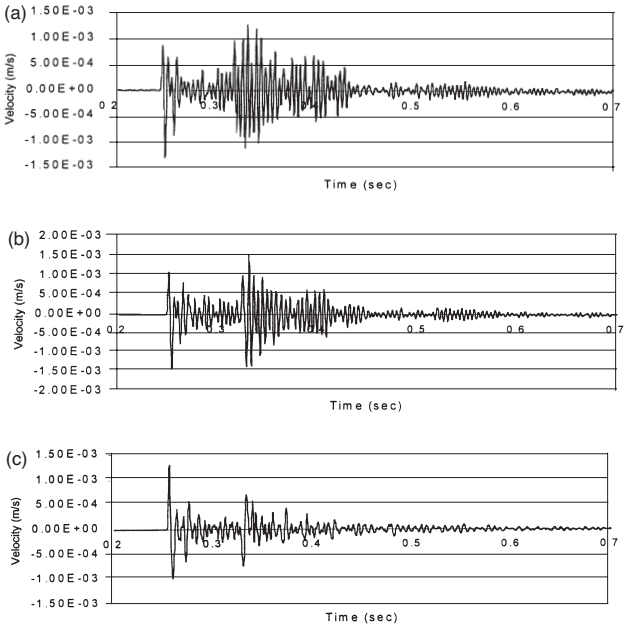

Figure 9 (a, b, c)—Three component seismogram of the blast recorded by the Klerksdorp regional seismic network by a station 850 m from the blast; a) is the horizontal component X, b) is the horizontal component Y and c) is the vertical component Z

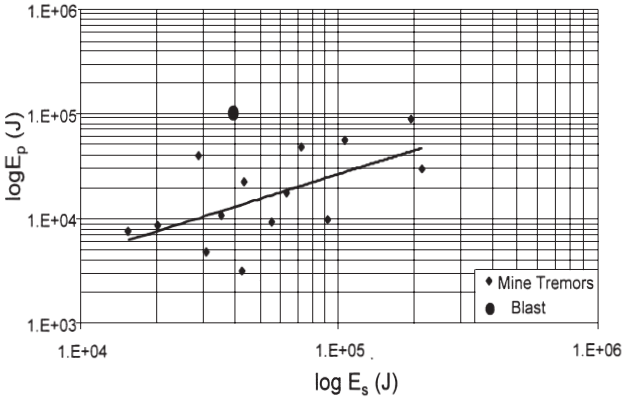

Figure 10—Energy emitted in P- waves versus energy emitted in S-waves from the simulated rockburst and 14 mine-induced seismic events located in the same portion of the mine

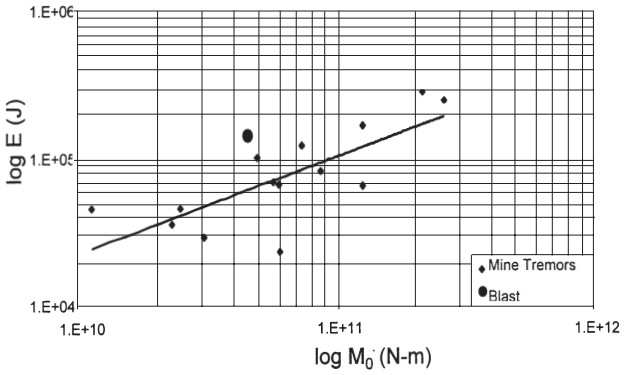

Figure 11—Energy versus moment for the simulated rockburst and 14 mine-induced seismic events located in the same portion of the mine

Seismic signal monitoring after the blast

Seismic data were collected before and after the blast. The sources were two blasting sequences located at two working faces at about 100 m from the test site (Figure 12). The standard production cartridges were used in these blasting sequences. The 'source-receiver' geometry allowed the seismic waves to propagate through the area affected by the blast. Previous work by Durrheim *et al.*[10] indicated that the amplification of the seismic signal on the skin of excavations is dependent on the degree of fragmentation in the vicinity of the receiver. These effects have been studied further using the data recorded before and after the blast.

A comparison of the peak particle velocities recorded before and after the blast indicated a five- to six-fold amplification of the velocities recorded after the blast (Figure 13).

In addition, a comparison was made between the geophone located closer to the blast and the geophone 12 m further away from the blast. The peak particle velocities recorded before the blast for both the close and the distant geophones were in the range of 0.1 mm/s to 1.0 mm/s. They did not differ significantly from each other. After the blast, the values of the peak particle velocities recorded on the closest geophone were 2 to 3 times higher than the velocities recorded at the distant geophone. This indicates an increase in fracture intensity close to the source. An increase of peak particle velocities increase of fracture intensity was also observed at Tau Tona mine by Milev *et al.*[12].

An amplification of the seismic signal recorded before and after the blast was obtained on the hangingwall and on the footwall. However, this amplification was not considered as a true representation of the rockmass behaviour as additional factors such as the remaining mesh and lacing on the hangingwall and the soft ground between the geophone and the footwall were influenced by the peak particle velocities. On the other hand, the presence of an amplification in the hangingwall and the footwall indicates that the seismic signal was amplified not only on the surface of the blasting wall but also during the propagation through the highly fragmented source region.

The results obtained so far indicate that there is significant amplification of the peak particle velocities when the seismic wave is propagating through the fractured rock. This analysis has profound implications that require further study.

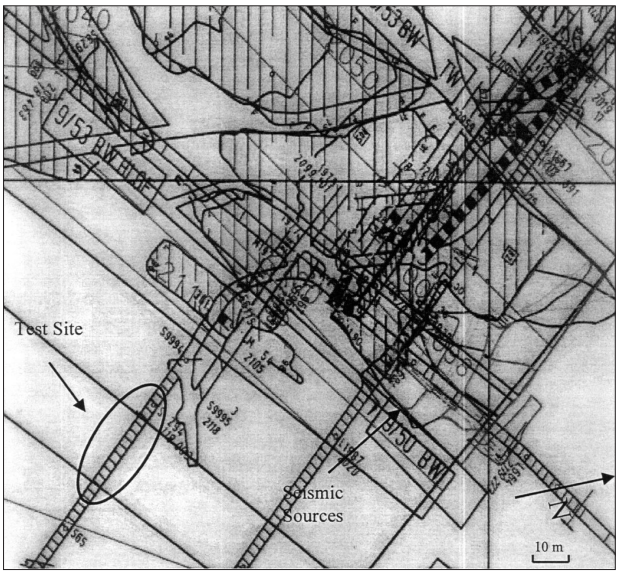

Figure 12—A plan of the test site

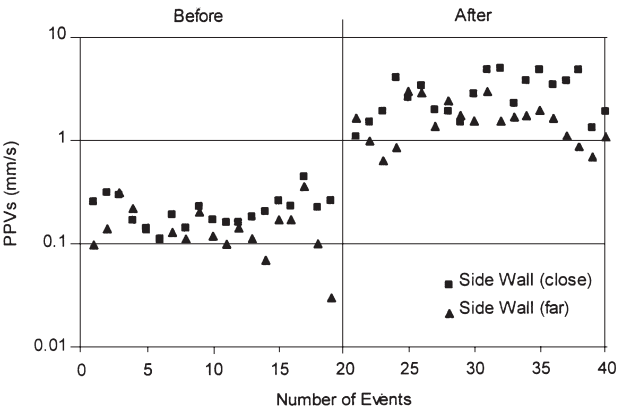

Figure 13—Peak particle velocities measured at the blasting site before the main blast and after the main blast

Conclusions

Some of the important findings are listed below:

- No gas pressure was directly involved in damaging the wall of the tunnel. The damage resulted from the interaction of the blast wave with the tunnel, as would happen in a rockburst.
- Two areas of damage were identified on the blasting wall:
  - an area of high-intensity damage: a ground velocity of 3.3 m/s was recorded by an accelerometer subsequently ejected in a block of rock; and
  - an area of low-intensity damage: a ground velocity of 1.6 m/s was recorded by an accelerometer which remained on the tunnel wall
- High-speed filming revealed rock fragments being ejected from the wall at velocities in the range of 0.6 m/s to 2.5 m/s. The measurements were taken in the area of low-intensity damage.
- The attenuation of peak particle velocities for the main blast, in the near field (6 m to 30 m) as a function of distance R, was found to follow the law of $R^{-1.7}$.
- The simulated rockburst was recorded as a local magnitude M_L = 1.3 by the Klerksdorp regional seismic network. Further use of the simulated rockburst for scaling of mine tremors located in this region is recommended.
- It was possible to measure the peak particle velocities (PPVs) on the tunnel wall both before and after the simulated rockburst. These PPVs were generated by ongoing mining operations some 100 m from the site. The PPVs after the blast were amplified some five to six times as a result of the damage caused to the rock surrounding the excavation.

Acknowledgements

The authors would like to express their thanks to SIMRAC for the financial support and to the GAPREAG committee for their encouragement. We would like also to thank the management, production and rock engineering staff of the Kopanang Mine for their assistance and co-operation at various stages of the simulated rockburst.

References

1. Roberts, M.K.C. Stope and Gully Support, SIMRAC Final Project Report GAP 030, Pretoria: Department of Minerals and Energy, 1995.
2. Jesenak, P., Kaiser, P.K., and Brummer, R.K. Rockburst damage potential assessment. *Proc. 3rd Int. Symp. on Rockbursts and Seismicity in Mines*: Rotterdam, Balkema, 1993. pp. 81–86.
3. Reddy, N. and Spottiswoode, S.M. The influence on geology on a simulated rockburst experiment. *The Journal of The South African Institute of Mining and Metallurgy*, 2001, submitted.
4. Hagan, T.O., Milev, A.M., Spottiswoode, S.M., Vakalisa, B., and Reddy, N. Improvement of worker safety through the investigation of the site response to rockbursts, SIMRAC Final Project Report GAP 530, Pretoria: Department of Minerals and Energy, 1998, 147 pp.
5. Hildyard, M.W. and Milev, A.M. Simulated rockburst experiment: Development of a numerical model for seismic wave propagation from the blast, and forward analysis. The Journal of The South African Institute of Mining and Metallurgy, 2001a, submitted.
6. Rorke, A.J. Measurement of the direct effects of preconditioning blasts. Monitored results from the first test blast. Internal report, prepared for Mr. D. Adams, COMRO, Ref: R62/92 Feb. 1992.
7. Ouchterlony, S.N., Nyberg, U., and Deng, J. Monitoring of large open cut rounds by VOD, PPV and gas pressure measurements. *Fragblast: International Journal of Blasting and Fragmentation*, vol. 1, no. 1, 1997. pp. 3–25.
8. Persson, P., Holmberg, R., and Lee, Y. *Rock blasting and explosives engineering*, CRC, Press, USA, 1990.
9. Haile, A.T. A mechanistic evaluation and design of tunnel support systems for deep level South African mines, Ph.D. thesis, Mechanical Engineering Dept., University of Natal, 1999, South Africa, 302 pp.
10. Durrheim, R.J., Milev, A.M., Spottiswoode, S.M., and Vakalisa, B. Improvement of worker safety through the investigation of the site response to rockbursts, SIMRAC Final Project Report GAP 201. Pretoria: Department of Minerals and Energy, 1997, 530 pp.
11. Spottiswoode, S.M., Durrheim R.J., Vakalisa, B., and Milev, A.M. 1997. Influence of fracturing and support on the site response in deep tabular stopes, *Proc. 1st SARES*, R.G. Gürtünca and T.O. Hagan (Editors), Johannesburg, pp. 62–68.
12. Milev, A.M., Spottiswoode, S.M., and Stewart, R.D. 1999. Dynamic response of the rock surrounding deep level mining excavations. *Proc. 9th ISRM*, G. Vonille and P. Berset (Editors), Paris'99, pp. 1109–1114. ◆